# PDZ Domains from the Junctional Proteins Afadin and ZO-1 Act as Mechanosensors

Vipul T. Vachharajani[1], Matthew P. DeJong[2], and Alexander R. Dunn[2, 3]

[1]Graduate Program in Biophysics, Stanford University, Stanford, CA 94305
[2]Department of Chemical Engineering, Stanford University, Stanford, CA 94305
[3]Cardiovascular Institute, Stanford University School of Medicine, Stanford, CA 94305

## Abstract

Intercellular adhesion complexes must withstand mechanical forces to maintain tissue cohesion, while also retaining the capacity for dynamic remodeling during tissue morphogenesis and repair. Most cell-cell adhesion complexes contain at least one PSD95/Dlg/ZO-1 (PDZ) domain situated between the adhesion molecule and the actin cytoskeleton. However, PDZ-mediated interactions are characteristically nonspecific, weak, and transient, with several binding partners per PDZ domain, micromolar dissociation constants, and bond lifetimes of seconds or less. Here, we demonstrate that the bonds between the PDZ domain of the cytoskeletal adaptor protein afadin and the intracellular domains of the adhesion molecules nectin-1 and JAM-A form molecular catch bonds that reinforce in response to mechanical load. In contrast, the bond between the PDZ3-SH3-GUK (PSG) domain of the cytoskeletal adaptor ZO-1 and the JAM-A intracellular domain becomes dramatically weaker in response to ~2 pN of load, the amount generated by single molecules of the cytoskeletal motor protein myosin II. These results suggest that PDZ domains can serve as force-responsive mechanical anchors at cell-cell adhesion complexes, and that mechanical load can enhance the selectivity of PDZ-peptide interactions. PDZ mechanosensitivity may thus help to generate the intricate molecular organization of cell-cell junctions and allow junctional complexes to dynamically remodel in response to mechanical load.

## Introduction

The construction of epithelial tissues requires the coordination of multiple classes of transmembrane adhesion molecules that bind across the cell-cell junction to connect neighboring cells (Fig. 1A)[1,2]. These linkages between cells must maintain robust adhesion in the face of mechanical forces due to both external stresses and cellular events such as division and death, while also maintaining the dynamic properties that make tissue remodeling and repair possible[3–5]. How these seemingly contradictory properties are achieved at the molecular level is in general poorly understood. Although previous studies have examined how the components of cadherin-mediated adherens junctions respond to mechanical load[6–13], much less is known about how the other adhesion complexes present at cell-cell junctions may respond to force[14].

Unlike the cadherin-catenin complex, most other cell-cell adhesion complexes contain a cytoskeletal linker protein containing at least one PDZ domain[1]. In general, PDZ domains bind to the C-terminal ~5 residues of multiple binding partners, resulting in a complex combinatorial network of PDZ-peptide interactions (Fig. 1B)[15–18]. Afadin and zonula occludens-1 and -2 (ZO-1/2) are PDZ containing scaffolding proteins that help to organize adherens and tight junctions at cell-cell contacts, respectively[1,19–22]. Both proteins bind transmembrane cellular adhesion proteins via their PDZ domains, and link directly to filamentous, (F)-actin, providing a potential conduit for force transmission between cell adhesion complexes and the actin cytoskeleton. ZO-1, afadin, and their binding partners are known to be mechanoresponsive, such that mechanical tension exerted at cell-cell junctions leads to altered intracellular signal transduction and

transcriptional regulation[14,23–25]. However, to our knowledge how and whether PDZ-mediated linkages by afadin, ZO-1, or any other protein may respond to mechanical load remains unexamined.

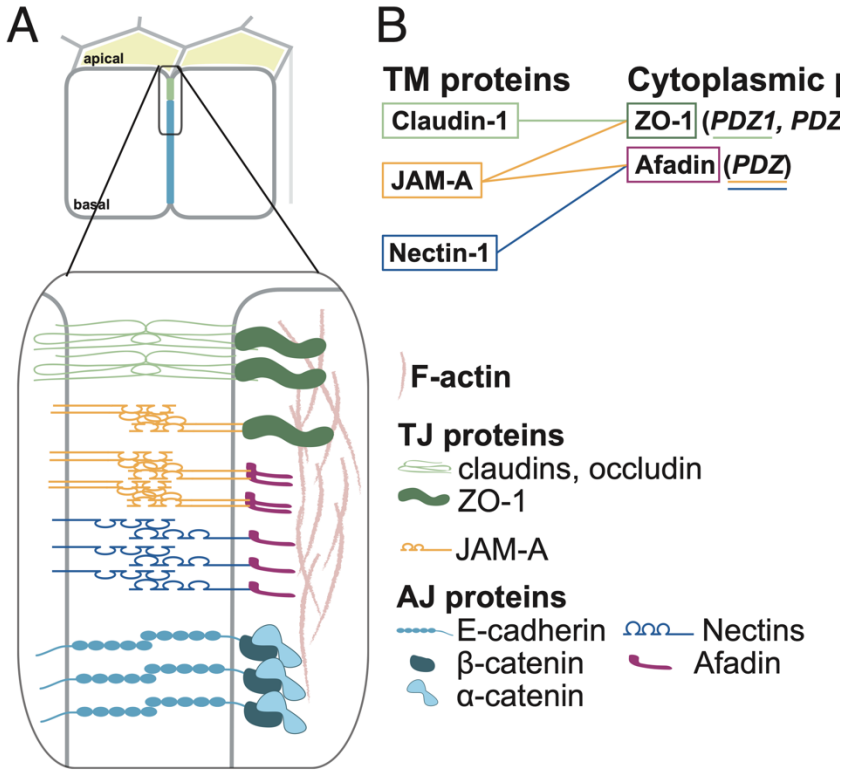


**Figure 1. Apicobasal organization of cell-cell junctions.** (A) Schematic showing the diversity of cell-cell adhesion molecules and intracellular scaffold proteins at the junction. Modified with permission from Vasquez, de la Serna, and Dunn (2021). (B) Network of PDZ-mediated interactions between transmembrane (TM) proteins and cytoplasmic partners.

The overlapping network of PDZ-peptide interactions at the cell junction raises a fundamental question of how the intricate organization of cell-cell junctions can arise from a network of overlapping interactions. Afadin possesses one PDZ domain, which can bind to either the JAM family of tight junction proteins or to the nectin family of adherens junction proteins[26,27]. ZO proteins have three PDZ domains. Of these, PDZ1 binds to claudins, while PDZ3 binds to JAMs[28–30]. Importantly, PDZ3 exists as part of structural module containing PDZ, Src homology 3 (SH3), and guanylate kinase (GUK) domains, termed the PSG module[29,31]. The ZO-1 PSG also forms a dense web of interactions with the cytoskeletal adaptor proteins afadin, αE-catenin, vinculin, and shroom2, signal transduction proteins such as ZONAB and $G\alpha_{12}$, and the tight junction protein occludin[23,31–39]. In addition to its central role in the construction of tight junctions, ZO-1 plays an integral role in the formation of new cell-cell contacts and is recruited to nascent adherens junctions through its interactions with afadin and αE-catenin[40–45]. The factors that regulate ZO-1 localization of tight vs. adherens junctions, and more broadly its interactions with a diverse array of binding partners, remain poorly understood.

## Results

*Nectin-1 and JAM-A form short-lived, μM-affinity bonds with the PDZ domain of afadin in solution.*

Unusually high affinities of the afadin PDZ domain for nectin and JAM-A could potentially explain the function of this linkage as a load-bearing linkage to the actin cytoskeleton. To directly measure affinities of afadin PDZ-binding ligands, we first measured the solution dissociation constants and binding kinetics of the intracellular domains (ICDs) of nectin-1 and JAM-A with the afadin PDZ domain (Fig. 2A, B, Supp. Fig. 1A, B). The affinity of the nectin-1 ICD with the afadin PDZ was approximately 3 μM as measured by both bio-layer interferometry (Fig. 2C) and fluorescence anisotropy (Supp. Fig. 2). The affinity of the JAM-A ICD and the afadin PDZ was likewise approximately 5 μM (Fig. 2C, Supp. Fig. 2), values that are consistent with previous measurements of PDZ-ligand dissociation constants.

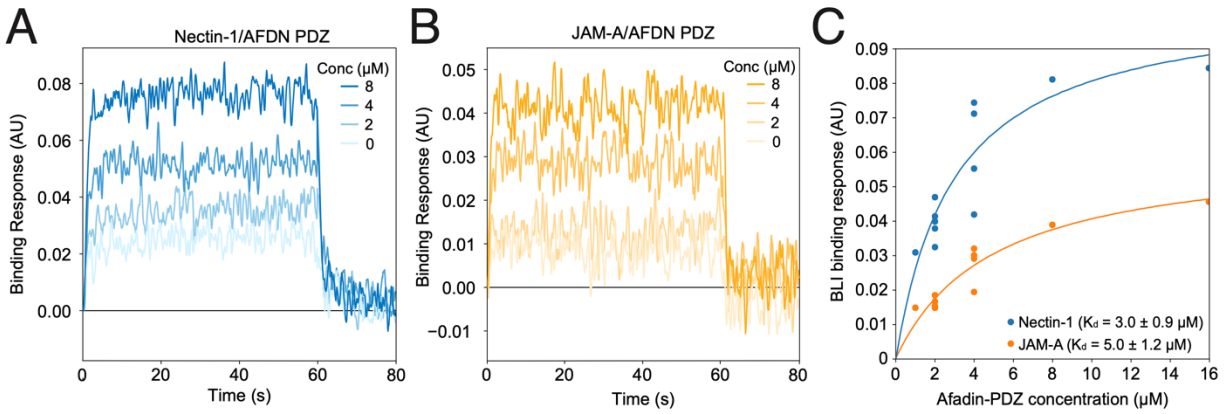


**Figure 2. JAM-A and nectin-1 ICDs have μM affinities for the Afadin PDZ and dissociate within seconds.** Representative BLI responses of (A) the nectin-1 ICD binding to the Afadin PDZ domain and (B) the JAM-A ICD binding to the afadin PDZ domain. (C) Equilibrium binding data for nectin-1 ICD/afadin PDZ and JAM-A ICD/Afadin PDZ indicate $K_D$ values of 3 and 5 μM, respectively.

We next tested the hypothesis that the bonds of the afadin PDZ to JAM-A, nectin-1, or both might be unusually long-lived. We measured binding kinetics using bio-layer interferometry and found that both ligands formed bonds with lifetimes on the single-second timescale, with bond lifetimes of 1.2 and 0.65 s for the nectin-1 and JAM-A ICDs, respectively (Fig. 2A, B, Supp. Fig. 1C). These relatively modest dissociation constants and bond lifetimes are striking given the hypothesized role of nectins in anchoring F-actin at cell-cell junctions[46–48]. In addition, the similarity in binding lifetimes suggests that it is unlikely that this provides a means by which afadin may distinguish between these two binding partners.

*Afadin-PDZ forms catch bonds with C-terminal ligands under force.*

We next used a single-molecule magnetic tweezer assay to measure single bond lifetimes at physiologically relevant, piconewton-scale forces. To do so, we designed a tethered-ligand construct in which the PDZ domain of afadin is linked to the C-terminal domain of either nectin-1 or JAM-A by a flexible glycine/serine linker, with handles for stable attachment on either side (Fig. 3A). These constructs were covalently attached on one end to a glass coverslip functionalized with a SpyCatcher-conjugated elastin-like polypeptide (ELP) and tethered to a 2.7 μm paramagnetic bead on the other end via a biotin-streptavidin interaction.

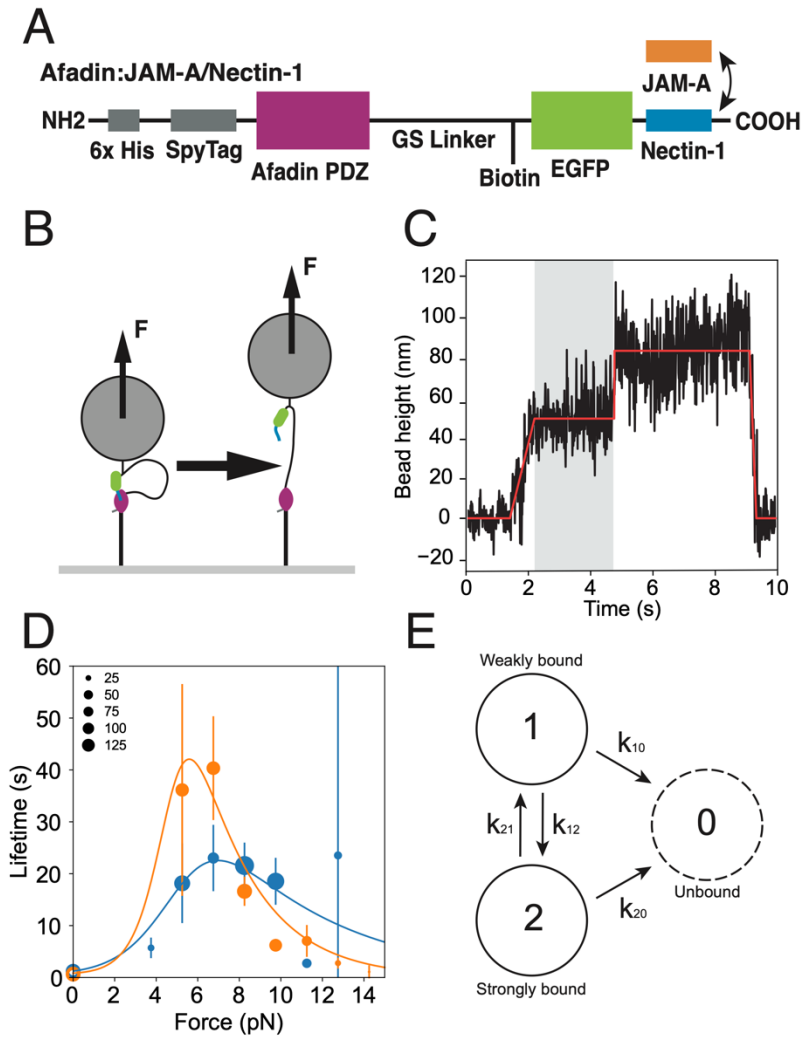


**Figure 3. A single-molecule magnetic tweezers assay to measure afadin PDZ unbinding kinetics under tension.** (A) Domain schematics for the magnetic tweezers afadin PDZ/nectin-1 or JAM-A fusion constructs. (B) Schematic of the force-jump magnetic tweezer experiment performed on tethered protein constructs. (C) Sample magnetic tweezer trace, plotting bead height vs. time. Actual data are shown in black, and a two-step fit is shown in red. The shaded region, during which force is applied but the linker has not extended, corresponds to the measured bond lifetime. (D) Average bond lifetime vs force for the nectin-1 ICD (blue, $N$ = 801) and JAM-A ICD (orange, $N$ = 567) constructs. Marker size corresponds to the number of observations. The open circles represent measured bond lifetimes at zero force from BLI. Filled circles correspond to means of 1.5-pN force bins. Two-state catch bond fits, constrained by the zero-force lifetime, are shown in solid lines for nectin-1/afadin and JAM-A/afadin. Error bars denote the standard deviation of bond lifetimes for each bin. (E) Kinetic schematic for the two-state catch bond. States 1 and 2 are the weakly and strongly bound states, respectively. State 0 is the unbound state. Rate constants $k_{12}$, $k_{10}$, and $k_{20}$ exponentially grow with force. The rate constant $k_{21}$ exponentially decays with force.

To test the hypothesis that force modulates afadin-PDZ bond kinetics, we performed force-jump experiments. Briefly, bead height was monitored as the force on the bead was increased from <1 pN to a fixed force between 3 and 15 pN. The time between the end of the initial force ramp and the steplike change in bead height corresponding to linker extension was taken as the bond lifetime (Fig. 3C). To confirm that the step we measured corresponded to the appropriate linker extension, we repeated the experiment using a construct containing a longer linker and observed a corresponding increase in step height (Supp. Fig. 3).

As force increased from 0, we observed an increase in bond lifetime up to a peak value around 5-7 pN for both nectin-1/afadin and JAM-A/afadin (Fig. 3D), after which point the bond lifetime decreased with increasing force. This behavior is consistent with the presence of a molecular catch bond, in which binding lifetimes increase over a given force range. To further characterize these force-lifetime measurements, we fit a two-state catch bond model to the data[49,50], using the measured zero-force lifetime as a fit constraint. In this model, the PDZ-peptide complex transitions between strong binding, weak binding, and unbound states (Fig. 3E). Mechanical load shifts the equilibrium toward the strong-binding state, thus increasing the average bound-state lifetime over the range of 0 to ~6 pN. Increasing load past ~6 pN accelerates dissociation from the strongly bound state, leading to a decrease in bound-state lifetimes. Fit parameters are listed in Table 1. These results suggest that afadin can form catch bonds with its C-terminal ligands, and thus stably associate with ligands under tension, despite its low affinity for these ligands in solution.

**Table 1. Maximum likelihood estimate parameters for kinetic models.** State 1 is the weakly bound state, state 2 is the strongly bound state, and state 0 is the unbound state. $k_{ij}^0$ is the zero-force transition rate between states *i* and *j*. $x_{ij}$ is the distance between state *i* and the transition state between *i* and *j*.

| **Afadin/Nectin-1** | | | | |
|---|---|---|---|---|
| | 1→0 | 2→0 | 1→2 | 2→1 |
| $k_{ij}^0$ (1/s) | 19 | 0.02 | 47000 | 6100 |
| $x_{ij}$ (nm) | 4.1 | 0.7 | 7.1 | -16 |
| **Afadin/JAM-A** | | | | |
| | 1→0 | 2→0 | 1→2 | 2→1 |
| $k_{ij}^0$ (1/s) | 2.2 | 0.003 | 15 | 32 |
| $x_{ij}$ (nm) | 2.4 | 1.5 | 6.0 | -1.6 |
| **ZO-1/JAM-A** | | | | |
| | 1→0 | | | |
| $k_{ij}^0$ (1/s) | 0.025 | | | |
| $x_{ij}$ (nm) | 10.3 | | | |

*Force accelerates the dissociation of the complex between the JAM-A ICD and the ZO-1 PSG domain.*

To assess how force selects for certain PDZ-peptide binding interactions, we measured JAMA-ICD dissociation from the ZO-1 PSG domain under force. We designed a tethered-ligand construct in which the PSG fragment of ZO-1 is linked to the C-terminal domain of JAM-A using the same linkers and handles as in the JAM-A/afadin PDZ measurements (Fig. 4A). We found that binding was reversible at low pN forces, so we performed force-clamp experiments to quantify bond lifetimes (Fig. 4C). Strikingly, we observed a strong monotonic decrease in bond lifetime to <0.1 s at 2.3 pN (Fig. 4D). These data are well described by a single-state slip bond, in which mechanical force accelerates dissociation from a single bound state (Fig. 4E). Fit parameters are listed in Table 1. The measured $x_{10}$, the distance to the transition state for the dissociation step, was 10.3 nm. This large distance implies a correspondingly large conformational rearrangement in the PSG during dissociation (see Discussion).

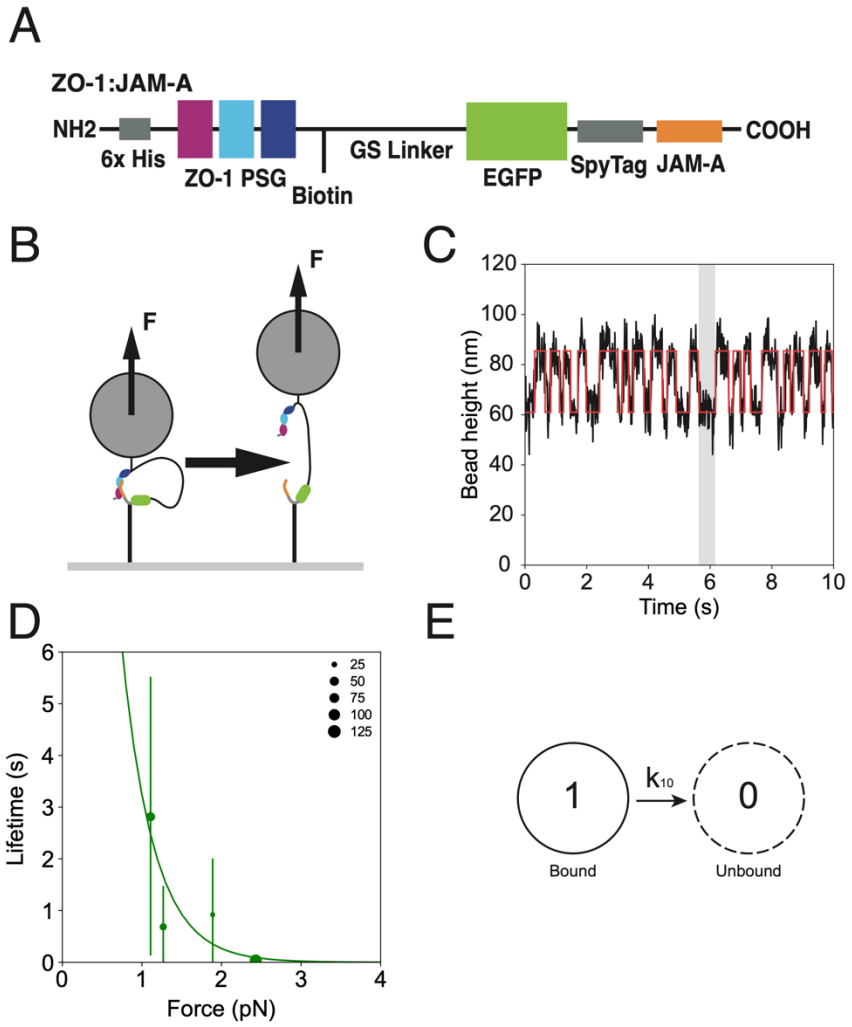


**Figure 4. A single-molecule magnetic tweezers assay to measure ZO-1 PSG unbinding kinetics under tension.** (A) Domain schematic for the magnetic tweezers ZO-1 PSG/JAM-A fusion construct. The ZO-1 PSG includes a PDZ domain (*pink*), an SH3 domain (*light blue*), and a GUK domain (*dark blue*). (B) Schematic of the force-clamp magnetic tweezer experiment performed on the tethered protein construct. (C) Sample magnetic tweezer trace, plotting bead height over time. Actual data are shown in *black*, and two-step fit in *red*. (D) Average bond lifetime vs force for JAM-A/ZO-1 ($N$ = 245). Marker size corresponds to the number of observations. A one-state slip bond fit is shown. Error bars denote standard deviation of bond lifetime for each bin. (E) Kinetic schematic for the one-state slip bond. State 1 is the bound state, and state 0 is the unbound state. The rate constant $k_{10}$ grows exponentially with force.

## Discussion

Our results demonstrate that the afadin PDZ domain forms strong bonds under tension with the ICDs of nectin-1 and JAM-A, despite its relatively weak affinity for both ligands in solution. In contrast, the ZO-1 PSG domain forms a remarkably force-sensitive slip bond with the JAM-A ICD. Thus, physiologically relevant forces can exert dramatic and opposite effects on the stability of two of the major linkages between cell-cell adhesion proteins and the F-actin cytoskeleton. Though we examined only two PDZ domains in detail, the abundance of PDZ domains present at cell-cell junctions suggests that PDZ-domain mechanosensitivity may represent a new class of mechanical behaviors that govern the organization and dynamics of cell adhesion ligands.

The two-state catch bond models for the dissociation of the afadin PDZ domain with the JAM-A and nectin-1 ICD peptides contain large distance parameters $x_{12}$ and $x_{21}$, implying that the afadin PDZ domain undergoes relatively large conformational changes under load. The nature of these implied structural transitions is unclear and constitutes an important target for future investigations. The large value of $x_{10}$ for the dissociation of the ZO-1 PSG and JAM-A ICD likewise implies that a large structural rearrangement is coupled to dissociation. Previous experiments demonstrate that both the PDZ and SH3 domains are required for detectable binding between the ZO-1 PSG and JAM-A ICD, and the structure of the complex reveals contacts between the JAM-A ICD and the SH3 domain[29]. A 39-residue disordered loop connects the SH3 and GUK domains. Extension of this loop and rotation of the GUK domain would yield an increase in overall length of ~15 nm, in good agreement with the 10 nm extension implied by the value of $x_{10}$. We speculate that undocking of the PDZ, SH3, and GUK domains precedes dissociation of the JAM-A ICD under load. If so, such a mechanism would explain the remarkable force sensitivity of the dissociation step.

It is likely that nectins play an important role in the initiation of new cell-cell contacts. Nectin *trans*-heterodimers have nM affinity[51,52], much stronger than the μM affinity of the cadherin extracellular domain[53]. This and other observations have led to the hypothesis that nectin- and afadin-based adhesions may form first and then template cadherin-based adhesions[33,46,54,55]. Our results suggest a potential mechanism by which initial nectin-only contacts may robustly recruit afadin to perform this role. Further experiments are necessary to more directly test the hypothesis that *trans*-interacting nectins and afadin bear tension in cells.

The nectin-afadin linkage may directly modulate afadin's regulatory functions in some tissues. Two nectinopathies have been identified in humans: a nectin-1 dominant negative mutation is associated with the cleft lip/palate-ectodermal dysplasia syndrome (CLPED), and a nectin-4 deletion in the afadin PDZ-binding C-terminus has been associated with an ectodermal dysplasia/cutaneous syndactyly syndrome (EDSS1)[56–60]. Furthermore, in a murine model, an afadin conditional knockout phenocopies a nectin-1/nectin-4 double knockout, resulting in the same phenotype as observed in humans with CLPED[61]. These results clearly identify the nectin-afadin linkage as instrumental to ectodermal morphogenesis, and it is intriguing to speculate that a PDZ catch bond may contribute to this important role.

A growing body of evidence implicates JAM-A in cellular mechanosensing[14,24,25]. In one such example, application of tension to the extracellular domain of JAM-A led to the activation of RhoA downstream of serine phosphorylation of the JAM-A ICD[24]. Other studies indicate that JAM-A indirectly regulates cytoskeletal contractility at cell-cell junctions through p114RhoGEF and PDZ-GEF1, and the G protein Rap2[25,62,63]. Understanding how these, and likely other, PDZ-mediated forms of mechanosensing contribute to junctional mechanotransduction offers a promising avenue for future investigations.

Our data motivate the hypothesis that PDZ-based mechanosensing may play an important and previously unrecognized role in regulating the dynamics and organization of cell-cell contacts. The formation of catch bonds between afadin and JAM-A and nectin provides an appealing means by which these adhesions can automatically reinforce to protect cell-cell junctions against disruption by mechanical load. Conversely, recent studies support a model in ZO-1 provides a liquid-like, fluid interface between tight junctions and F-actin[64]. Our data suggest that the ZO-1-JAM-A linkage is particularly sensitive to applied force, analogous to shear-thinning liquids whose viscosity decreases in response to applied load. Finally, we note that the relative affinities of, for example, JAM-A for ZO-1 and afadin are predicted to vary dramatically as a

function of mechanical load. We therefore propose that mechanical force may play a key role in regulating the complex web of interactions that underlie the intricate organization of epithelial cell-cell junctions.

**Acknowledgements**
V.T.V. is supported by the Stanford Medical Scientist Training Program (NIH T32GM007365) and the NIH NIDDK (1F30DK124985). M.P.D is supported by the NSF Graduate Research Fellowship (DGE-1656518). A.R.D. acknowledges the HHMI (Faculty Scholar Award) and the NIH (R35GM130332) for funding that supported this research.

## Methods

### Plasmids, protein expression, and purification

A plasmid encoding the GST-tagged human afadin PDZ domain was a gift from Sachdev Sidhu (Addgene plasmid # 103938 ; http://n2t.net/addgene:103938 ; RRID:Addgene_103938). Plasmids encoding tethered fusion constructs were custom cloned by Epoch Biosciences (Missouri City, TX). Proteins were expressed in *E. coli* BL21(DE3) chemically competent cells (New England Biolabs). Cultures of 500 mL in LB broth were induced at OD 0.6 with 1mM IPTG at 18 °C overnight. The cultures were then spun down at 6000×G for 30 minutes.

For GST-tagged proteins, bacterial pellets were resuspended in PBS pH 7.5 with a cOmplete EDTA-free protease inhibitor cocktail (11873580001, Roche), 70 µg/mL lysozyme (90082, ThermoFisher), and 7 U/mL DNase I (04536282001, Roche). The resuspended cells were rotated end-over-end for 30 min at 4 °C, lysed with a tip sonicator, and spun at 12,000×G for 30 minutes to pellet bacterial cell debris. The supernatant was clarified by filtering through a 0.44 ×G µm PVDF syringe filter and then incubated with 2 mL of Pierce glutathione agarose resin (16100, ThermoFisher) for 2 hr at 4 °C in a 5 mL polypropylene column. The resin was washed with four column volumes of PBSTR buffer (PBS, 1M NaCl, 0.005% Tween-20, 1mM DTT) followed by four column volumes of HRV-3C protease cleavage buffer. The column was stopped, and one column volume of cleavage buffer added along with 6x His-tagged HRV-3C protease (kind gift from Elise Bruguera, Stanford University) to remove the GST tag. The column was capped and rotated overnight at 4 °C and the eluate collected. The eluate was incubated with Ni:NTA coated magnetic beads (MyOne HisPur, ThermoFisher) and separated with a magnet to remove residual 3C protease, and then concentrated using a 3 kDa MWCO spin column (Amicon). Protein was divided into 20 µL aliquots, flash frozen in liquid nitrogen, and stored at -80 °C until use.

For His-tagged proteins, pelleted cells were resuspended lysis buffer (50 mM sodium phosphate, 300 mM NaCl, and 10 mM imidazole, pH 8) with cOmplete EDTA-free protease inhibitor cocktail (11873580001, Roche), 70 µg/mL_lysozyme (90082, ThermoFisher), and 7 U/mL DNase I (04536282001, Roche). Cells were lysed and the lysate clarified as above, then incubated with 2 mL HisPur resin at 4 °C for 2 hours. The solution was then packed into a gravity column, washed three times with 5 mL of wash buffer (50 mM sodium phosphate, 300 mM NaCl, and 20 mM imidazole, pH 7.4 with 2 mM β-mercaptoethanol; BME), and protein was eluted by incubating the resin bed with 1 mL of elution buffer (50 mM sodium phosphate, 300 mM sodium chloride, and 250 mM imidazole, pH 7.4 and 2 mM BME) for 5 minutes, four times. The eluate was collected, concentrated, and buffer-exchanged into storage buffer (phosphate-buffered saline, 2 mM BME) using Amicon centrifugal filter units (MilliporeSigma) of the appropriate molecular-weight cutoff, then flash-frozen and stored at −80 °C.

### Zero-force binding assays

All binding experiments were performed in buffer containing 50 mM HEPES, 150 mM NaCl, 1 mg/mL Bovine Serum Albumin, and 0.02% Tween-20 at pH 7.5.

*Protein expression and purification*
The C-terminal 10mer peptides of nectin-1 and JAM-A (sequences in Supplementary Table 1) were purchased lyophilized from Genscript with N-terminal biotinylation and N-terminal FITC

conjugation. nectin-1 peptide was redissolved at 1 mg/mL concentration in MilliQ water; JAM-A peptide was redissolved at 10mg/mL in anhydrous DMSO.

*Bio-layer interferometry*
Bio-layer interferometry was conducted using the GatorPrime instrument (Gator Bio, Palo Alto, CA), using streptavidin-coated probes. Probes were loaded with 100 ng/mL biotinylated peptide for 4 min, then equilibrated in buffer for 10 minutes. Binding kinetics were measured at various concentrations of afadin PDZ using an association phase of 300 s and a dissociation phase of 600 s after dipping into fresh wells of buffer. Repeated association and dissociation curves were obtained sequentially from the same probe at 2 mM and 4 mM concentrations. Experiments were repeated on three separate days with separate probes. A blank probe without peptide was used to correct for nonspecific adsorption of PDZ to the probe.

*Fluorescence anisotropy*
Fluorescence anisotropy was measured on a BioTek Synergy 2 plate reader. Briefly, FITC-labeled peptide at a final concentration of 50 ng/mL was mixed with the afadin PDZ domain of varying concentrations in black low-binding 96-well plates (Costar).

**Magnetic tweezers**

*Construction and calibration*
A magnetic tweezer was constructed on a Nikon Ti-E microscope equipped with a motorized 3-axis piezo stage (Mad City Labs). Two 6 mm-diameter cylindrical shaped N52 magnets were affixed to a custom-fabricated aluminum bracket, which was attached to a 0.5”-travel XYZ translation stage equipped with a motorized Z-axis actuator (Thorlabs, Newton, New Jersey, USA). The stage position was homed before measurement by stepping the Z-actuator until the magnet bracket just touched the top of the sample. Measurements were performed while the Nikon Perfect Focus feedback system was turned on.

Samples were illuminated from the objective side via a mint green LED (Thorlabs) reflected into the back focal plane of a 100x Plan-Apo TIRF objective using a polarizing beamsplitter (Edmund Optics). Reflected cross-polarized light was transmitted through the beamsplitter and collected by an sCMOS camera (Hamamatsu Orca Flash v4). Bead images were collected using a custom-written LabView script or MicroManager 1.4 software[65].

Magnetic tweezers force calibration was performed as described previously[66] using transverse fluctuations of a magnetic bead tethered to a glass coverslip via lambda phage DNA (New England Biolabs).

*Data analysis*
A nonspecifically adhered bead was used to generate a reference image lookup table (LUT) while the piezo stage was stepped in increments of 10 nm. These LUTs were used to estimate the *z*-position of a query bead image. Briefly, the two-dimensional Fourier transform of the query bead image was calculated, and the radial profile extracted. The bead position was then estimated as follows: The one-dimensional Fourier transform of the LUT radial profiles was computed. The phase of the highest-amplitude frequency was then plotted against the bead height corresponding to the LUT slice, and a third-order polynomial was fit to this curve. This polynomial fit was then used to directly estimate height from the Fourier transform of the query image. Images were analyzed with both methods and found to produce similar results, reducing the chance that measured bead heights were analysis artifacts.

*Sample preparation*
SpyCatcher-ELP-functionalized #1.5 glass coverslips were prepared as previously described[67], and stored in vacuum-sealed boxes at -20 °C. Briefly, 3-5 mm wide slits were cut with a razor blade into a piece of Parafilm M (Bemis) and sandwiched between a glass slide (1 mm thick, Fisher Scientific) and a SpyCatcher-ELP coverslip, to produce channels of ~20 microliter volume. The assembly was heated on a 60 °C hot plate for 1 minute in increments of 15 seconds to adhere the parafilm to the glass. Channels were passivated overnight in blocking buffer (1 mg/mL Casein and 0.1% (v/v) Tween-20 in PBS). Samples were then washed with 10 channel volumes of assay buffer (50mM HEPES, 150 mM NaCl, pH 7.5) and incubated with 100 pM to 10 nM biotinylated fusion protein, for 1.5 hours. Samples were then washed with 10 channel volumes of buffer again, and then incubated with 1:10 M270-Streptavidin superparamagnetic beads diluted in blocking buffer for 25 minutes. Samples were then washed a final time with 10 channel volumes of assay buffer before measurement.

*Force-jump experiments*
Force jump experiments were performed as follows: A suitable bead tethered by a single complex was identified by comparing its force-extension behavior to that of the ELP, and centered in the microscope field of view. The magnetic tweezer was kept fully retracted from the coverslip, corresponding to sub-pN forces.

In each cycle, the magnet was quickly lowered to a set value while the bead height was monitored. Once the target height was reached, the magnet was held in place until the bead height exceeded a set threshold, at which point the magnet was then fully raised. Between cycles, the magnet was kept at maximum height for 30 seconds to allow the complex to return to binding equilibrium.

Extension traces over time for the force-jump cycles were analyzed as follows: a single-step profile with linear loading and unloading steps was fit with a least-squares objective function for each trace using the NumPy SHGO constrained global optimization routine, from which the bond lifetime and step size were measured. Traces were manually inspected to retain only those for which the pre-extension of the ELP handle was between 30 and 60 nm, and for which a step unbinding was clearly visible by eye.

*Force-clamp experiments*
Force-clamp experiments were performed following the force-jump protocol with the modification that instead of cycling the magnet position, the magnet position was held in a fixed position to obtain constant-force measurements.

*Catch bond model fitting*
Bond lifetimes were fit to a two-state catch bond model[49,50] as follows. An initial fit was obtained using the NumPy Dual Annealing routine to maximize likelihood. The SHGO constrained global optimization routine was then used to minimize negative log likelihood, while allowing each parameter to vary up to 10-fold about the initial fit. Model fits were constrained such that the zero-force lifetime was equal to that measured by BLI.

## References


1. Rouaud, F. *et al.* Scaffolding proteins of vertebrate apical junctions: structure, functions and biophysics. *Biochim Biophys Acta Biomembr* **1862**, 183399 (2020).
2. Vasquez, C. G., de la Serna, E. L. & Dunn, A. R. How cells tell up from down and stick together to construct multicellular tissues - interplay between apicobasal polarity and cell-cell adhesion. *J Cell Sci* **134**, jcs248757 (2021).
3. Collins, C. & Nelson, W. J. Running with neighbors: coordinating cell migration and cell-cell adhesion. *Curr Opin Cell Biol* **36**, 62–70 (2015).
4. Clarke, D. N. & Martin, A. C. Actin-based force generation and cell adhesion in tissue morphogenesis. *Curr Biol* **31**, R667–R680 (2021).
5. Yap, A. S., Duszyc, K. & Viasnoff, V. Mechanosensing and Mechanotransduction at Cell-Cell Junctions. *Cold Spring Harb Perspect Biol* **10**, a028761 (2018).
6. Yonemura, S., Wada, Y., Watanabe, T., Nagafuchi, A. & Shibata, M. alpha-Catenin as a tension transducer that induces adherens junction development. *Nat. Cell Biol.* **12**, 533–542 (2010).
7. Buckley, C. D. *et al.* Cell adhesion. The minimal cadherin-catenin complex binds to actin filaments under force. *Science* **346**, 1254211 (2014).
8. Wang, A., Dunn, A. R. & Weis, W. I. Mechanism of the cadherin-catenin F-actin catch bond interaction. *Elife* **11**, e80130 (2022).
9. Bax, N. A. *et al.* Multi-level Force-dependent Allosteric Enhancement of αE-catenin Binding to F-actin by Vinculin. *J Mol Biol* **435**, 167969 (2023).
10. Borghi, N. *et al.* E-cadherin is under constitutive actomyosin-generated tension that is increased at cell-cell contacts upon externally applied stretch. *Proc Natl Acad Sci U.S.A.* **109**, 12568–12573 (2012).
11. Röper, J.-C. *et al.* The major β-catenin/E-cadherin junctional binding site is a primary molecular mechano-transductor of differentiation in vivo. *Elife* **7**, e33381 (2018).
12. Oldenburg, J. *et al.* VASP, zyxin and TES are tension-dependent members of Focal Adherens Junctions independent of the α-catenin-vinculin module. *Sci Rep* **5**, 17225 (2015).
13. Ishiyama, N. *et al.* Force-dependent allostery of the α-catenin actin-binding domain controls adherens junction dynamics and functions. *Nat Commun* **9**, 5121 (2018).
14. Citi, S. The mechanobiology of tight junctions. *Biophys Rev* **11**, 783–793 (2019).
15. Kim, J. *et al.* Rewiring of PDZ domain-ligand interaction network contributed to eukaryotic evolution. *PLoS Genet* **8**, e1002510 (2012).
16. Stiffler, M. A. *et al.* PDZ domain binding selectivity is optimized across the mouse proteome. *Science* **317**, 364–369 (2007).
17. Sundell, G. N. *et al.* Proteome-wide analysis of phospho-regulated PDZ domain interactions. *Mol Syst Biol* **14**, e8129 (2018).
18. Ivarsson, Y. *et al.* Large-scale interaction profiling of PDZ domains through proteomic peptide-phage display using human and viral phage peptidomes. *Proc Natl Acad Sci U S A* **111**, 2542–2547 (2014).
19. Togashi, H. Differential and Cooperative Cell Adhesion Regulates Cellular Pattern in Sensory Epithelia. *Front Cell Dev Biol* **4**, 104 (2016).
20. Lechuga, S. & Ivanov, A. I. Disruption of the epithelial barrier during intestinal inflammation: Quest for new molecules and mechanisms. *Biochim Biophys Acta Mol Cell Res* **1864**, 1183–1194 (2017).
21. Buckley, C. E. & St Johnston, D. Apical-basal polarity and the control of epithelial form and function. *Nat Rev Mol Cell Biol* **23**, 559–577 (2022).
22. Otani, T. & Furuse, M. Tight Junction Structure and Function Revisited. *Trends Cell Biol* **30**, 805–817 (2020).

23. Spadaro, D. *et al.* Tension-Dependent Stretching Activates ZO-1 to Control the Junctional Localization of Its Interactors. *Curr Biol* **27**, 3783-3795.e8 (2017).
24. Scott, D. W., Tolbert, C. E. & Burridge, K. Tension on JAM-A activates RhoA via GEF-H1 and p115 RhoGEF. *Mol Biol Cell* **27**, 1420–1430 (2016).
25. Haas, A. J. *et al.* Interplay between Extracellular Matrix Stiffness and JAM-A Regulates Mechanical Load on ZO-1 and Tight Junction Assembly. *Cell Rep* **32**, 107924 (2020).
26. Tachibana, K. *et al.* Two cell adhesion molecules, nectin and cadherin, interact through their cytoplasmic domain-associated proteins. *J Cell Biol* **150**, 1161–1176 (2000).
27. Ebnet, K., Schulz, C. U., Meyer Zu Brickwedde, M. K., Pendl, G. G. & Vestweber, D. Junctional adhesion molecule interacts with the PDZ domain-containing proteins AF-6 and ZO-1. *J Biol Chem* **275**, 27979–27988 (2000).
28. Nomme, J. *et al.* The Src homology 3 domain is required for junctional adhesion molecule binding to the third PDZ domain of the scaffolding protein ZO-1. *J Biol Chem* **286**, 43352–43360 (2011).
29. Nomme, J. *et al.* Structural Basis of a Key Factor Regulating the Affinity between the Zonula Occludens First PDZ Domain and Claudins. *J Biol Chem* **290**, 16595–16606 (2015).
30. Itoh, M. *et al.* Direct binding of three tight junction-associated MAGUKs, ZO-1, ZO-2, and ZO-3, with the COOH termini of claudins. *J Cell Biol* **147**, 1351–1363 (1999).
31. Lye, M. F., Fanning, A. S., Su, Y., Anderson, J. M. & Lavie, A. Insights into regulated ligand binding sites from the structure of ZO-1 Src homology 3-guanylate kinase module. *J Biol Chem* **285**, 13907–13917 (2010).
32. Mattagajasingh, S. N., Huang, S. C., Hartenstein, J. S. & Benz, E. J. Characterization of the interaction between protein 4.1R and ZO-2. A possible link between the tight junction and the actin cytoskeleton. *J Biol Chem* **275**, 30573–30585 (2000).
33. Ooshio, T. *et al.* Involvement of the interaction of afadin with ZO-1 in the formation of tight junctions in Madin-Darby canine kidney cells. *J Biol Chem* **285**, 5003–5012 (2010).
34. Zemljic-Harpf, A. E. *et al.* Vinculin directly binds zonula occludens-1 and is essential for stabilizing connexin-43-containing gap junctions in cardiac myocytes. *J Cell Sci* **127**, 1104–1116 (2014).
35. Müller, S. L. *et al.* The tight junction protein occludin and the adherens junction protein alpha-catenin share a common interaction mechanism with ZO-1. *J Biol Chem* **280**, 3747–3756 (2005).
36. Itoh, M., Nagafuchi, A., Moroi, S. & Tsukita, S. Involvement of ZO-1 in cadherin-based cell adhesion through its direct binding to alpha catenin and actin filaments. *J Cell Biol* **138**, 181–192 (1997).
37. Etournay, R. *et al.* Shroom2, a myosin-VIIa- and actin-binding protein, directly interacts with ZO-1 at tight junctions. *J Cell Sci* **120**, 2838–2850 (2007).
38. Meyer, T. N., Schwesinger, C. & Denker, B. M. Zonula occludens-1 is a scaffolding protein for signaling molecules. Galpha(12) directly binds to the Src homology 3 domain and regulates paracellular permeability in epithelial cells. *J Biol Chem* **277**, 24855–24858 (2002).
39. Tash, B. R. *et al.* The occludin and ZO-1 complex, defined by small angle X-ray scattering and NMR, has implications for modulating tight junction permeability. *Proc Natl Acad Sci U S A* **109**, 10855–10860 (2012).
40. Lockwood, C., Zaidel-Bar, R. & Hardin, J. The C. elegans zonula occludens ortholog cooperates with the cadherin complex to recruit actin during morphogenesis. *Curr Biol* **18**, 1333–1337 (2008).
41. Yokoyama, S. *et al.* alpha-catenin-independent recruitment of ZO-1 to nectin-based cell-cell adhesion sites through afadin. *Mol Biol Cell* **12**, 1595–1609 (2001).

42. Itoh, M., Nagafuchi, A., Moroi, S. & Tsukita, S. Involvement of ZO-1 in cadherin-based cell adhesion through its direct binding to alpha catenin and actin filaments. *J Cell Biol* **138**, 181–192 (1997).
43. Ando-Akatsuka, Y., Yonemura, S., Itoh, M., Furuse, M. & Tsukita, S. Differential behavior of E-cadherin and occludin in their colocalization with ZO-1 during the establishment of epithelial cell polarity. *J Cell Physiol* **179**, 115–125 (1999).
44. Yamazaki, Y. *et al.* ZO-1- and ZO-2-dependent integration of myosin-2 to epithelial zonula adherens. *Mol Biol Cell* **19**, 3801–3811 (2008).
45. Ikenouchi, J., Umeda, K., Tsukita, S., Furuse, M. & Tsukita, S. Requirement of ZO-1 for the formation of belt-like adherens junctions during epithelial cell polarization. *J Cell Biol* **176**, 779–786 (2007).
46. Sato, T. *et al.* Regulation of the assembly and adhesion activity of E-cadherin by nectin and afadin for the formation of adherens junctions in Madin-Darby canine kidney cells. *J Biol Chem* **281**, 5288–5299 (2006).
47. Troyanovsky, R. B., Indra, I., Chen, C.-S., Hong, S. & Troyanovsky, S. M. Cadherin controls nectin recruitment into adherens junctions by remodeling the actin cytoskeleton. *J Cell Sci* **128**, 140–149 (2015).
48. Indra, I., Hong, S., Troyanovsky, R., Kormos, B. & Troyanovsky, S. The Adherens Junction: A Mosaic of Cadherin and Nectin Clusters Bundled by Actin Filaments. *J Invest Dermatol* **133**, 2546–2554 (2013).
49. Barsegov, V. & Thirumalai, D. Dynamics of unbinding of cell adhesion molecules: transition from catch to slip bonds. *Proc Natl Acad Sci U S A* **102**, 1835–1839 (2005).
50. Thomas, W. *et al.* Catch-bond model derived from allostery explains force-activated bacterial adhesion. *Biophys J* **90**, 753–764 (2006).
51. Ikeda, W. *et al.* Tage4/Nectin-like molecule-5 heterophilically trans-interacts with cell adhesion molecule Nectin-3 and enhances cell migration. *J Biol Chem* **278**, 28167–28172 (2003).
52. Rikitake, Y., Mandai, K. & Takai, Y. The role of nectins in different types of cell-cell adhesion. *J Cell Sci* **125**, 3713–3722 (2012).
53. Chappuis-Flament, S., Wong, E., Hicks, L. D., Kay, C. M. & Gumbiner, B. M. Multiple cadherin extracellular repeats mediate homophilic binding and adhesion. *J Cell Biol* **154**, 231–243 (2001).
54. Tanaka, Y. *et al.* Role of nectin in formation of E-cadherin-based adherens junctions in keratinocytes: analysis with the N-cadherin dominant negative mutant. *Mol Biol Cell* **14**, 1597–1609 (2003).
55. Takai, Y. & Nakanishi, H. Nectin and afadin: novel organizers of intercellular junctions. *J Cell Sci* **116**, 17–27 (2003).
56. Brancati, F. *et al.* Mutations in PVRL4, encoding cell adhesion molecule nectin-4, cause ectodermal dysplasia-syndactyly syndrome. *Am J Hum Genet* **87**, 265–273 (2010).
57. Yoshida, K. *et al.* Novel homozygous mutation, c.400C>T (p.Arg134*), in the PVRL1 gene underlies cleft lip/palate-ectodermal dysplasia syndrome in an Asian patient. *J Dermatol* **42**, 715–719 (2015).
58. Brancati, F., Agolini, E. & Fortugno, P. Nectinopathies: an emerging group of ectodermal dysplasia syndromes. *G Ital Dermatol Venereol* **148**, 59–64 (2013).
59. Jelani, M., Chishti, M. S. & Ahmad, W. Mutation in PVRL4 gene encoding nectin-4 underlies ectodermal-dysplasia-syndactyly syndrome (EDSS1). *J Hum Genet* **56**, 352–357 (2011).
60. Fortugno, P. *et al.* Nectin-4 mutations causing ectodermal dysplasia with syndactyly perturb the rac1 pathway and the kinetics of adherens junction formation. *J Invest Dermatol* **134**, 2146–2153 (2014).
61. Lough, K. J. *et al.* Disruption of the nectin-afadin complex recapitulates features of the human cleft lip/palate syndrome CLPED1. *Development* **147**, dev189241 (2020).

62. Monteiro, A. C. *et al.* JAM-A associates with ZO-2, afadin, and PDZ-GEF1 to activate Rap2c and regulate epithelial barrier function. *Mol Biol Cell* **24**, 2849–2860 (2013).
63. Tornavaca, O. *et al.* ZO-1 controls endothelial adherens junctions, cell-cell tension, angiogenesis, and barrier formation. *J Cell Biol* **208**, 821–838 (2015).
64. Beutel, O., Maraspini, R., Pombo-García, K., Martin-Lemaitre, C. & Honigmann, A. Phase Separation of Zonula Occludens Proteins Drives Formation of Tight Junctions. *Cell* **179**, 923-936.e11 (2019).
65. Edelstein, A. D. *et al.* Advanced methods of microscope control using μManager software. *J Biol Methods* **1**, e10 (2014).
66. Adhikari, A. S., Chai, J. & Dunn, A. R. Multiplexed single-molecule force proteolysis measurements using magnetic tweezers. *J Vis Exp* (2012) doi:10.3791/3520.
67. Brian L. Zhong, Vipul T. Vachharajani, & Alexander R. Dunn. STReTCh: a strategy for facile detection of mechanical forces across proteins in cells. *Cell Rep. Meth.* **2**, 100278 (2022).